The natural History of 'Oumuamua

Bannister, M., Bhandare, A., Dybczynski, P., Fitzsimmons, A., Guilbert-Lepoutre, A., Jedicke, R., Knight, M., Meech, K. J., McNeill, A., Pfalzner, S., Raymond, S., Snodgrass, C., Trilling, D., & Ye, Q. (2019). The natural History of 'Oumuamua. *Nature Astronomy*. Advance online publication. https://doi.org/10.1038/s41550-019-0816-x

Published in:
Nature Astronomy

Document Version:
Peer reviewed version

Draft version March 22, 2019
Typeset using LaTeX default style in AASTeX62

The Natural History of ‘Oumuamua

The ‘Oumuamua ISSI Team

(Received January 31, 2019; Revised March 22, 2019)

Submitted to Nature Astronomy

ABSTRACT

The discovery of the first interstellar object (ISO) passing through the Solar System, 1I/2017 U1 (‘Oumuamua), provoked intense and continuing interest from the scientific community and the general public. The faintness of ‘Oumuamua, together with the limited time window within which observations were possible, constrained the information available on its dynamics and physical state. Some authors have speculated that some features of this remarkable object point to an artificial nature, but “extraordinary claims require extraordinary evidence”[a)]. We address these arguments, and find that in all cases the observations are consistent with a purely natural origin for ‘Oumuamua. We discuss how the observed characteristics of ‘Oumuamua are explained by our extensive knowledge of natural minor bodies in our Solar System and our current knowledge of the evolution of planetary systems. We highlight several areas requiring further investigation.

1. WHAT WE KNOW ABOUT ‘OUMUAMUA

1I/‘Oumuamua was discovered on 2017 October 19 in the w_{PS1}-band observations of the PanSTARRS1 (PS1) Near Earth Object survey (Meech et al. 2017). ‘Oumuamua was discovered three days after its closest approach to Earth at 0.16 au, well after it had passed closest to the Sun on 2017 September 9 at a perihelion distance of 0.25 au. By October 22 there was sufficient astrometry to securely identify that the orbit was hyperbolic (Meech et al. 2017) and the unique and unusual orbit was highlighted in the discovery announcements (Williams et al. 2017b,a). Because of its rapid motion, there was only a short interval during which observations were possible. Within a week the brightness had dropped by a factor of 10 and within a month by a factor of 100. We summarize the measured properties of ‘Oumuamua in Table 1.

The average brightness measured in visible wavelengths during the week after its discovery gave H_V=22.4 (Meech et al. 2017; Jewitt et al. 2017), providing the first indication that ‘Oumuamua has a radius in the hundred-meter range. *Spitzer Space Telescope* observations in the infrared on November 21–22 did not detect ‘Oumuamua (Trilling et al. 2018). Their upper limits on the flux imply an effective radius between 49–220 m, depending on the assumed surface properties. For surface scattering parameters (called beaming parameters) that are typical of comets, this implies an effective radius of 70 m and a geometric albedo of 0.1.

Very few minor planets this small have been as well characterized physically, which hampers aspects of direct comparison of ‘Oumuamua with similar objects from the Solar System. ‘Oumuamua is smaller than the smallest well-characterized comet nucleus by a factor of ∼3–10 (e.g., 103P/Hartley 2 by *EPOXI*, equivalent radius 0.58 km; A’Hearn et al. 2011). The main comparison targets are in the near-Earth asteroid population. Several sub-km asteroids have been visited by spacecraft; among the smallest intensively studied asteroids not visited by a spacecraft is the 57-meter radius (54509) YORP (Lowry et al. 2007; Taylor et al. 2007).

Several teams obtained photometric and spectral data in the optical to near-infrared to characterize ‘Oumuamua’s surface composition. ‘Oumuamua is red, similar to many Solar System small bodies, e.g., comets, D-type asteroids, some Jupiter Trojans, and the more neutral trans-Neptunian objects (Masiero 2017; Meech et al. 2017; Jewitt et al. 2017; Ye et al. 2017; Bannister et al. 2017; Fitzsimmons et al. 2018; Bolin et al. 2018). Published measurements give a red slope at optical wavelengths of ∼10–20%/100 nm. While the color is consistent with organic-rich surfaces, it is also

[a)] Sagan (1979) reformulated a well-established idea in science, e.g., Laplace (1812): “Plus un fait est extraordinaire, plus il a besoin d’être appuyé de fortes preuves ; car, ceux qui l’attestent pouvant ou tromper ou avoir été trompés, ces deux causes sont d’autant plus probables que la réalité du fait l’est moins en elle-même.”

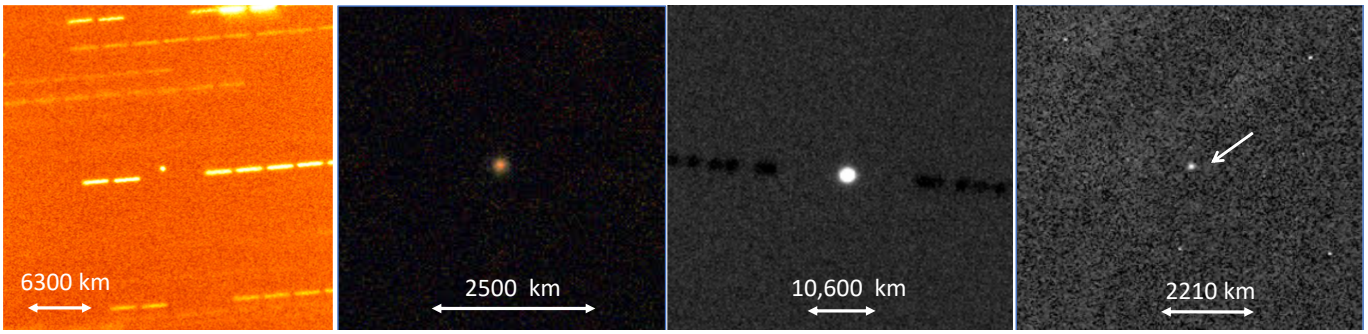

Figure 1. Montage of images of ‘Oumuamua showing its point-like unresolved appearance with no hint of detectable activity. From left to right: 0.4 hr integration through an R-band filter with the Nordic Optical Telescope on 2017 October 26 (Jewitt et al. 2017); “true color” image simulated from *griz*Y-band images obtained on 2017 October 27 for a total integration of 1.6 hr with the Gemini South telescope (Meech et al. 2017); a deep 3.6 hr *r*-band composite image obtained on 2017 October 27-28 with the Gemini North telescope (Drahus et al. 2018); and an F350LP image from *Hubble Space Telescope* (Micheli et al. 2018).

consistent with iron-rich minerals, and with space weathered surfaces (Moretti et al. 2007). Thus, color alone is not diagnostic of composition. Comparing the published spectroscopic and photometric data implies that some spectral variability with rotational phase is plausible within the data’s uncertainties, but not certain (Fitzsimmons et al. 2018; Fraser et al. 2018). As albedo and spectral variability do not necessarily correlate, this does not imply any albedo variation, although it cannot be ruled out.

‘Oumuamua exhibited short-term brightness variation of over a factor of ten (>2.5 magnitudes; Meech et al. 2017; Knight et al. 2017; Jewitt et al. 2017; Bannister et al. 2017; Bolin et al. 2018). The brightness range was unusually large. Of the minor planets in our Solar System with well-quantified light curves, there are only a handful of asteroids with brightness variations of this scale (Warner et al. 2009; last updated 31 January 2019). In most cases, these particularly high-amplitude light curves are based on observations of sub-100 m near-Earth asteroids at high phase angles, or on fragmentary light curves of slow-rotating objects.

While brightness variations can be due to variations in the viewing geometry of a particular shape, or due to patchy albedo across a surface, minor planets’ light curves are usually assumed to be shape-dominated, as their surfaces are thought to be covered by small regolith that is evenly distributed across the surface (Fujiwara et al. 2006; Polishook et al. 2014). ‘Oumuamua’s light curve shape, with narrow “V-shaped” minima and broad maxima, is indicative that its large brightness variations are caused by its shape, rather than variations in its albedo (Lacerda & Jewitt 2007). Both phase angle and rotation state need to be considered in understanding ‘Oumuamua’s shape. Only a limited range of phase angles (19–27°) could be observed in the short time span during which observations useful for defining ‘Oumuamua’s rotation were made. Accounting for the known effect of the enhancement of amplitude with increasing phase angle (Zappala et al. 1990), McNeill et al. (2018) inferred that the true ratio of longest axis to shortest axis is ≥6:1. Due to the unknown orientation of ‘Oumuamua’s rotation pole, this axial ratio represents only a lower limit.

‘Oumuamua’s brightness varied on a timescale of about 4 hours (implying a rotation period of ∼8 hours for a double-peaked lightcurve), but the various teams did not converge on a consistent rotation period while it was visible. Analysis of the full photometric data set showed that ‘Oumuamua was in a state of excited rotation (Fraser et al. 2018; Drahus et al. 2018; Belton et al. 2018). The most comprehensive model published to date (Belton et al. 2018) concluded that ‘Oumuamua is rotating around its shortest axis with a period of 8.67±0.34 hours, and has a likely period of rotation around the long axis of 54.48 hours. How we interpret the shape of ‘Oumuamua depends on its specific state of rotation, including its rotation pole. ‘Oumuamua can either have a narrow elongated-ellipsoid shape or a shape more reminiscent of a flattened oval.

Sensitive searches for activity (Fig. 1) showed no evidence for micron-sized dust near ‘Oumuamua (Meech et al. 2017; Jewitt et al. 2017; Ye et al. 2017; Micheli et al. 2018). However, the observations were not sensitive to the detection of millimeter-sized and larger dust, so we have no constraints for the presence of large grains. There was also no detection of any gas, including searches for CN, H_2O, CO and CO_2 (Ye et al. 2017; Fitzsimmons et al. 2018; Park et al. 2018; Trilling et al. 2018), although the level to which each gas can be ruled out varies significantly.

A detailed investigation of the astrometric position measurements from the first observations in mid-October 2017 through the last observations obtained by the *Hubble Space Telescope* on January 2, 2018, showed that a gravity-only

Table 1. A summary of measured properties of 'Oumuamua

Quantity		Value	References
Dynamical Properties			
Perihelion distance	q [au]	0.255912 ± 0.000007	[1]
Eccentricity	e	1.20113 ± 0.00002	[1]
Incoming radiant	α, δ [deg]	279.4752, 33.8595	[11]
Earth close approach	Δ [au]	0.16175 ± 0.00001	[1]
Incoming velocity	v_∞ [km s^{-1}]	26.4204 ± 0.0019	[11]
Non-grav acceleration	$A_1 r^{-2}$ [m s^{-2}]	$(4.92 \pm 0.16) \times 10^{-6}$	[10]
Physical Properties			
Absolute magnitude	H_V	22.4 ± 0.04	[2]
Albedo	p_V	> [0.2,0.1,0.01]	[12]
Effective diameter	D_N [m]	<[98,140,440]	[12]
Rotation state		complex, long-axis mode	[5, 6, 7]
Rotation period	P [hr]	8.67 ± 0.34 hr (long-axis precess)	[6]
Axis ratio	a:b	>6:1	[8]
Shape		cigar, or oblate spheroid	[6]
Spectral slope	S_V [% per 100 nm]	23±3, 10±6, 9.3–17	[2, 3, 4]
Surface spectral type		D-type	[2, 4]
H_2O production	$Q(H_2O)$ [molec s^{-1}]	4.9×10^{25} @ 1.4 au (model)	[10]
OH production	Q(OH) [molec s^{-1}]	$< 1.7 \times 10^{27}$ @ 1.8 au (obs)	[9]
Hyper volatile (CO?)	Q(X) [molec s^{-1}]	4.5×10^{25} @ 1.4 au (model)	[10]
CO_2 production	$Q(CO_2)$ [molec s^{-1}]	$< 9 \times 10^{22}$ @ 2.0 au (obs)	[12]
CO production	Q(CO) [molec s^{-1}]	$< 9 \times 10^{23}$ @ 2.0 au (obs)	[13]
CN production	Q(CN) [molec s^{-1}]	$< 2 \times 10^{22}$ @ 1.4 au (obs)	[3]
C_2 production	$Q(C_2)$ [molec s^{-1}]	$< 4 \times 10^{22}$ @ 1.4 au (obs)	[3]
C_3 production	$Q(C_3)$ [molec s^{-1}]	$< 2 \times 10^{21}$ @ 1.4 au (obs)	[3]
Dust production	Q(dust) [kg s^{-1}]	$< 1.7 \times 10^{-3}$ @ 1.4 au (obs)	[2]
		< 10 @ $\sim 10^3$ au (obs)	[3]

†Reference Key: [1] JPL Horizons orbital solution #16; [2] Meech et al. (2017); [3] Ye et al. (2017); [4] Fitzsimmons et al. (2018); [5] Fraser et al. (2018); [6] Belton et al. (2018); [7] Drahus et al. (2018); [8] McNeill et al. (2018); [9] Park et al. (2018); [10] Micheli et al. (2018); [11] Bailer-Jones et al. (2018) using the pure $1/r^2$ radial acceleration solution from [10]; [12] Trilling et al. (2018); [13] M. Mommert (priv. comm.) revising the calculation in [12].

orbit provided an inadequate fit to the data. Instead, the data were well fit with the addition of a radial acceleration varying as $1/r^2$ (Micheli et al. 2018), where r is the heliocentric distance. This type of acceleration is frequently used in orbital studies of comets, and usually interpreted as being due to an activity-driven cometary acceleration consistent with the decreasing energy with distance from the Sun.

2. A CRITICAL REVIEW OF CURRENT THEORIES

The detection of interstellar objects (ISOs) was anticipated for decades (e.g. McGlynn & Chapman 1989; Kresak 1992; Cook et al. 2016; Engelhardt et al. 2017), due to the cohesive understanding of how planetary systems form and evolve (§ 2.1). However, some of the specifics of 'Oumuamua challenge aspects of planetary system theory. In the following subsections, we assimilate the various published ideas and show that 'Oumuamua's properties can be explained naturally.

2.1. *'Oumuamua Originated in a Planetary System*

A number of processes have been invoked to explain 'Oumuamua's origins and peculiarities since its discovery (Fig. 2; see also § 3.1). These models generally expect 'Oumuamua or its parent body to have been born as a planetary building block – a *planetesimal* – in a gas-dominated protoplanetary disk around a young star. Planetary disks containing

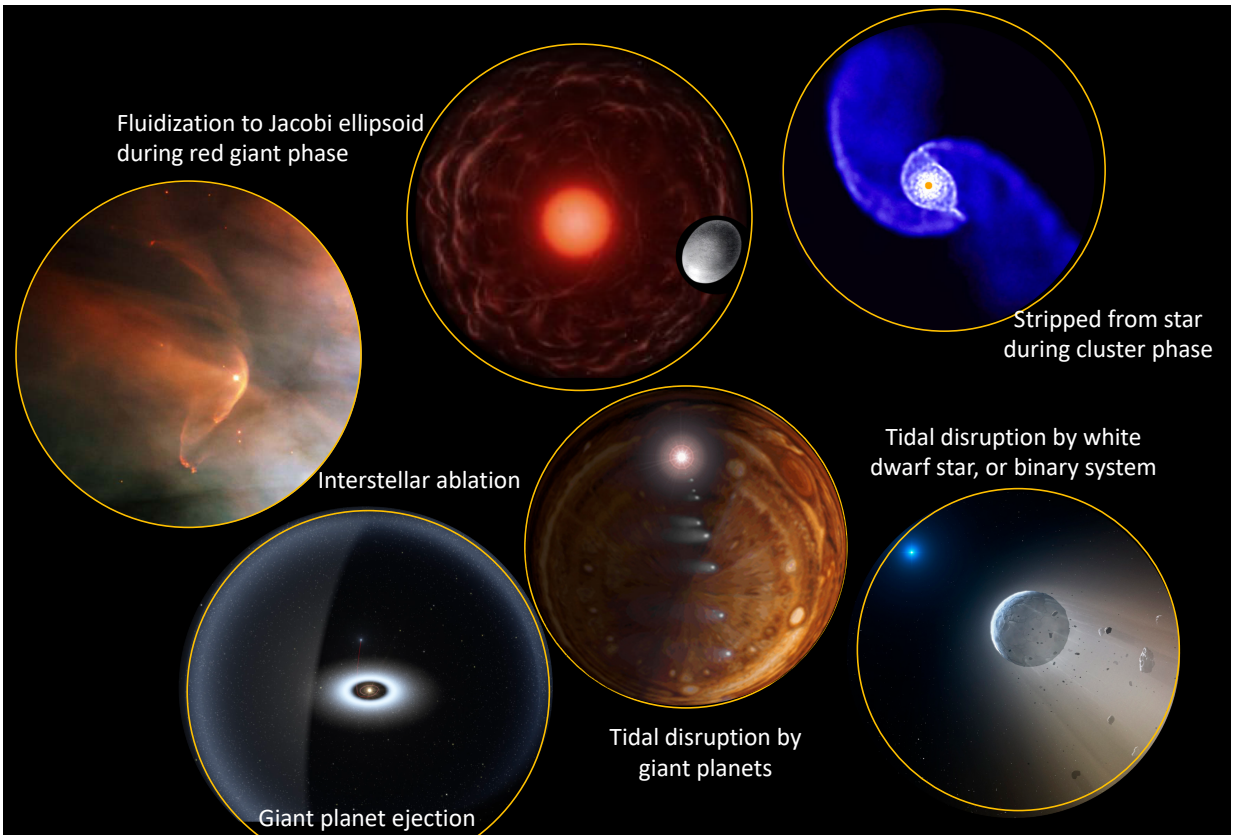

Figure 2. Montage of potential formation scenarios of 'Oumuamua as a natural planetesimal. Exact scenarios and their authoring papers are discussed in § 2.1 and § 3.1.

planetesimals are common around very young stars (< 3 Myr; Haisch et al. 2001; Hernández et al. 2008; Pfalzner et al. 2014). Roughly 20% of slightly older Sun-like stars are observed to still have mid-infrared excess emission (Trilling et al. 2008; Montesinos et al. 2016), interpreted as the dust generated by colliding outer planetesimals ("debris disks"; Wyatt 2008; Krivov 2010). This implies that a large fraction of stars are indeed born with large reservoirs of planetesimals capable of being dynamically ejected.

A straightforward explanation for 'Oumuamua is that it is a planetesimal (or a planetesimal fragment) ejected from its home system (Raymond et al. 2018b,a). During planetary system formation, a significant portion of a system's planetesimals are ejected into interstellar space (Charnoz & Morbidelli 2003; Raymond & Izidoro 2017). Gravitational interactions with the stars of the surrounding cluster or with the giant planets of the planetary system itself are major mechanisms of ejection (Tremaine 1993; Ford & Rasio 2008). For the latter, simulations show that planetesimals are most efficiently ejected in systems in which the giant planets themselves become unstable (Raymond et al. 2010). Binary star systems are as common as single stars; their planet formation is thought to proceed in a similar way (Thebault & Haghighipour 2015), and it seems that exoplanets are as common around binaries as single stars (Roell et al. 2012). In close binary systems (with a planet-forming disk exterior to two stars), planetesimals that enter within a critical distance to the binary are destabilized (Holman & Wiegert 1999) and quickly ejected as ISOs (Jackson et al. 2018). Close stellar flybys, which are common during the $\sim 3-5$ Myr-long embedded cluster phase (Adams et al. 2006; Vincke & Pfalzner 2016), can strip planetesimals from the outer parts of planetary systems (Pfalzner et al. 2005; Bhandare et al. 2016; Hands et al. 2019). As their host stars evolve off the main sequence and lose mass, planetesimals will eventually also be liberated from their home systems (Veras et al. 2011; Veras 2016).

2.2. *The Expected Number Density of Interstellar Objects in Space*

Combining the observed absolute magnitude of 'Oumuamua with current sky-survey detection limits, the number density of objects in interstellar space of the same size as 'Oumuamua or larger is about 0.1 au^{-3} (Meech et al. 2017; Trilling et al. 2017; Do et al. 2018). This estimate applies to objects with little to no activity (like 'Oumuamua)

and implies that interstellar objects are continuously passing through the Solar System below our current detection threshold.

It has been asserted that this number density of ISOs is 2–8 orders of magnitude higher than would be expected from planet formation scenarios (Bialy & Loeb 2018). However, transforming a number density of ISOs to a mass density requires a knowledge of the population's size-frequency distribution (SFD; e.g. Moro-Martín et al. 2009). With a single detected object there are no firm constraints on this distribution: until the ISO SFD is known from tens of detections, there is a disconnect between the measured number density of ISOs and their mass density.

We show with a simple experiment that the expected number density of ISOs varies by many orders of magnitude depending on the SFD applied to the mass (Fig. 3). Our estimate is based on the idea that 'Oumuamua is a planetesimal (or a planetesimal fragment) that was ejected from its home system by giant planets (see Raymond et al. 2010, 2018b, and § 2.1).

We first estimate the underlying mass density of ISOs based on planet formation theory and observational constraints. The density and mass distribution of stars are well-known (Kroupa et al. 1993; Bovy 2017); they are dominated by low-mass stars, with a Galactic disk-averaged value of ∼0.2 stars per cubic parsec. Virtually all stars host planets (Cassan et al. 2012). Radial velocity surveys find that ∼10–20% of Sun-like stars have gas giants (Mayor et al. 2011) but this fraction drops significantly for low-mass stars (Johnson et al. 2007; Lovis & Mayor 2007). The stellar mass-averaged frequency of gas giants is ∼1–10% (Winn & Fabrycky 2015). Microlensing surveys find that the occurrence rate of ice giants is significantly higher (∼10–50%) and has a weaker stellar mass dependence (Suzuki et al. 2016; Clanton & Gaudi 2016). Similarly, the ubiquity of gap structures in the ALMA disks suggests that Neptune-mass planets are common at large distances, with an occurrence rate estimated at ∼50% (Zhang et al. 2018).

How much mass in planetesimals does each system eject? This depends on the dynamics of each individual system and whether the planets remain stable (Raymond et al. 2010). We assume that each gas giant system ejects 1–100 Earth masses (Raymond et al. 2010). The abundant ice giants also efficiently eject planetesimals during (Izidoro et al. 2015) and after (Tremaine 1993) their formation; we assume each ice giant system ejects 0.1–10 Earth masses. Allowing for the frequency of the types of planetary systems, this comprises 0.1–10 Earth masses per star ejected by gas giants and 0.01–5 Earth masses by ice giants. This totals 0.02 to 15 Earth masses in ISOs per star or 0.004 to 3 Earth masses per cubic parsec.

We then calculate the expected number density of ISOs from that mass density estimate. Figure 3 shows the huge diversity of number densities of ISOs that can be inferred: the differences arise purely from the choice of plausible size-frequency distribution (SFD). While the uncertainty in our estimate of ejected planetesimal mass per star spans three orders of magnitude, the difference in inferred number density between SFDs is even larger (Fig. 3). For example, a power-law distribution characteristic of planetesimal formation simulations (SFD a_1) requires an implausibly large amount of mass – thousands of Earth masses – to be ejected per star in order to match the observational constraint on the number density (Raymond et al. 2018b; Rafikov 2018; Moro-Martín 2018, 2019a). However, several SFDs from Fig. 3 with somewhat more mass in small objects (e.g., SFD b_2 has 3% by mass in fragments and is otherwise similar to SFD a_1) can match the measured ISO number density. It is easier to match the inferred number density at the higher end of our estimate of the ISO mass density, but the main uncertainty comes from the assumed SFD.

Thus, given that the number density of ISOs cannot yet be reliably related to the mass density, the claim that the observed number density is presently "higher than expected" from planet formation scenarios is not supported.

2.3. *Uniqueness of the Trajectory*

While not typical for field stars, 'Oumuamua's trajectory is exactly what was expected for detectable ISOs (Engelhardt et al. 2017). As they age, stars in the solar neighbourhood are perturbed away from the Local Standard of Rest (LSR), which is defined by the galactic motions of nearby stars (Coşkunoğlu et al. 2011). Of course, a small fraction of older stars may still have small random velocities (Burgasser et al. 2015). 'Oumuamua's random velocity is 9 km s^{-1} from the LSR, far smaller than the ∼50 km s^{-1} velocity dispersion of nearby stars (Anguiano et al. 2018). This small random velocity could imply that 'Oumuamua is dynamically young (Meech et al. 2017), with a statistically-derived dynamical age of <2 Gyr (Portegies Zwart et al. 2018; Almeida-Fernandes & Rocha-Pinto 2018).

Gravitational focusing by the Sun creates an observational bias that favors the detection of ISOs with low random velocities, like that of 'Oumuamua (Engelhardt et al. 2017). This means it is challenging to use 'Oumuamua's galactic motion to constrain the ISO population's velocity dispersion. Indeed, as demonstrated in Figure 4, there appears to be nothing unusual about the specific parameters of 'Oumuamua's hyperbolic trajectory, as its perihelion

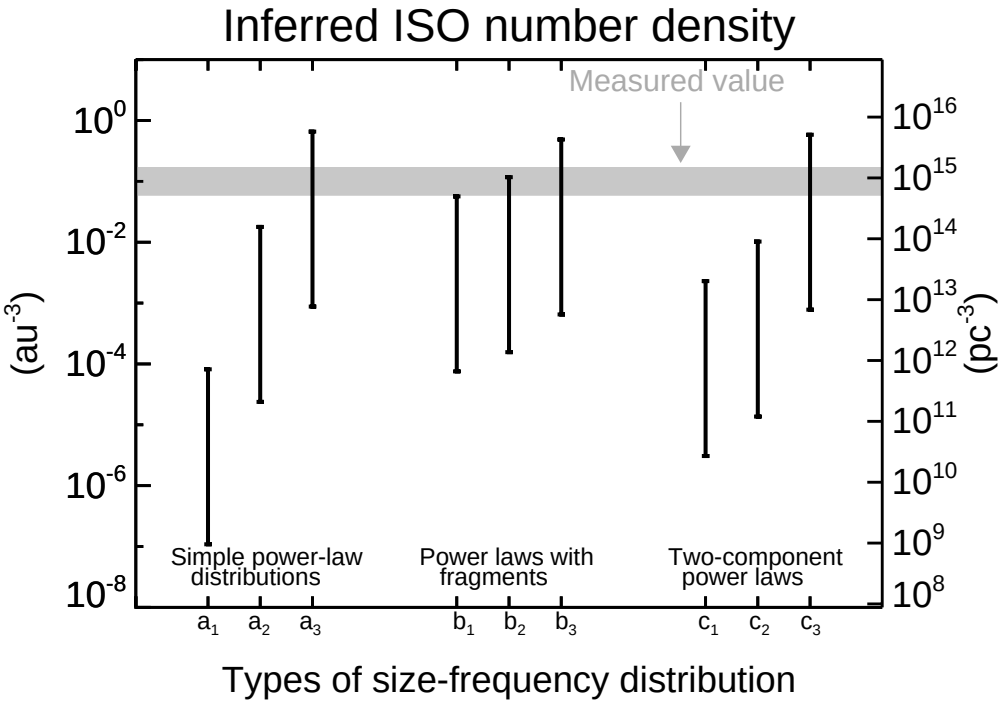

Figure 3. Inferred number density of ISOs – for a fixed estimate of the mass density of 0.004–3 Earth masses per cubic parsec – assuming different underlying size-frequency distributions (SFDs). We tested three SFDs: 1) power laws (a_{1-3}) in which the number of objects N of a given mass m is $N(m) \propto m^{-x}$; 2) power laws in which a small fraction (typically 1%) of the mass has been converted into fragments – comparable in size to 'Oumuamua, perhaps due to tidal disruption from giant planet encounters prior to ejection (Raymond et al. 2018b,a) (b_{1-3}); and 3) two-component power laws (c_{1-3}). The power laws extend from effective radii r_{min} to r_{max} with $N(m) \propto m^{-x}$, and all three have $r_{max} = 100$ km. Distribution a_1 is consistent with simulations of planetesimal formation (Simon et al. 2017; Schäfer et al. 2017) and has $r_{min} = 100$ m and $x = 0.6$. Distribution a_2 assumes collisional equilibrium (Dohnanyi 1969) and has $r_{min} = 50$ m and $x = 5/6$. Distribution a_3 is bottom-heavy (the smallest objects dominate by mass); it extrapolates the size-frequency distribution of boulders on comet 67P/Churyumov-Gerasimenko (Pajola et al. 2015) to large sizes and has $r_{min} = 50$ m and $x = 1.2$. Distribution b_1 contains 99% of its mass following distribution a_2 with 1% by mass in 50 m-sized fragments. Distribution b_2 contains 97% of its mass following distribution a_1 and 3% in 50 m-sized fragments (see Raymond et al. 2018b). Distribution b_3 is a single-size distribution, assuming that all ISOs are 'Oumuamua-sized (100 m). Distributions c_1 through c_3 all assume $r_{min} = 50$ m and $r_{max} = 100$ km. Distribution c_1 has $x = 0.6$ for objects larger than $r_{break} = 1$ km and $x = 5/6$ for smaller ones. Distribution c_2 has the same power laws but with $r_{break} = 10$ km. Distribution c_3 has $x = 0.6$ for objects larger than $r_{break} = 10$ km and $x = 1.2$ for smaller ones.

distance, eccentricity, and inclination agree well with the predicted distribution of the values for ISOs detectable by the major contemporary asteroid surveys — a prediction published (Engelhardt et al. 2017) nearly eight months *before* 'Oumuamua was discovered!

2.4. *"Cometary" Activity and Retention of Volatile Materials*

The mass loss needed to explain 'Oumuamua's observed non-gravitational acceleration is on the order of 1 kg s^{-1} (Micheli et al. 2018). Outgassing models for an object the size of 'Oumuamua with comet-like properties can produce this amount of mass loss at the distances observed (Cowan & A'Hearn 1979; Meech & Svoren 2004). Furthermore, when the *Rosetta* observations of comet 67P/Churyumov-Gerasimenko (made at comparable heliocentric distances to when 'Oumuamua was observed) are scaled down to an 'Oumuamua-sized object, they yield a similar outgassing rate (Pätzold et al. 2018). Depending on the assumptions, the total mass lost during the interval of observations represents ∼10% of 'Oumuamua's total mass (e.g., Seligman et al. 2019).

A typical comet with this level of outgassing would produce dust of all sizes, and no dust was detected. The absence of a radiation-pressure-swept tail indicates that if any particles were released, the effective particle size must be large. Observations by both ground-based telescopes and space missions to comets have shown that the ejection of

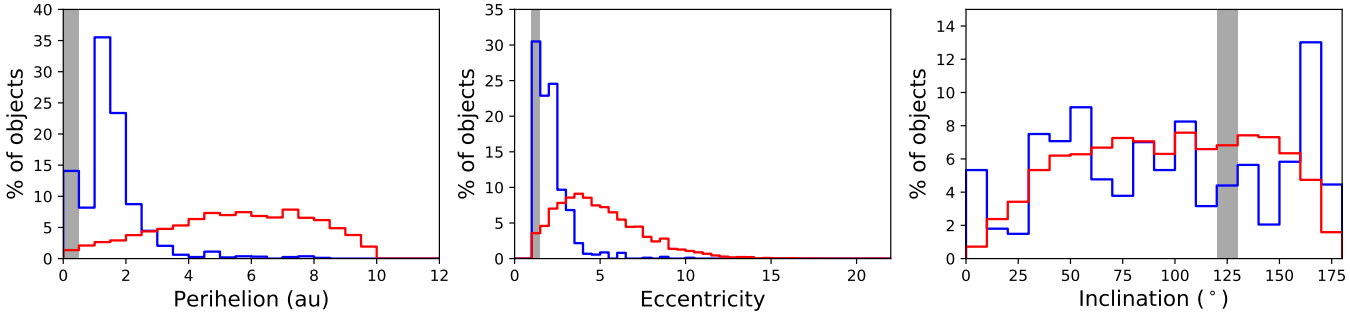

Figure 4. Predicted distribution of orbital elements of natural interstellar objects (blue curves are inactive objects, red curves are active objects) detected by the primary contemporary asteroid surveys (adapted from Engelhardt et al. 2017). In each distribution, ‘Oumuamua (gray vertical bar) has orbital elements at or near the most likely orbital elements.

fine-grained dust, which dominates the reflected light at visible wavelengths, is not always correlated with gas release. For example, comet 2P/Encke reaches a similar perihelion distance as ‘Oumuamua, and it often lacks any detectable dust at visible wavelengths (A’Hearn et al. 1995; Reach et al. 2000; Lisse et al. 2004). Some long-period comets preferentially eject large particles due to a mechanism that is currently not understood (Sekanina 1982; Ye & Hui 2014; Jewitt et al. 2018). Unfortunately, no observations were sensitive to large dust grains, which are most detectable in radio wavelengths, and meteor observations (sensitive to 0.1–1 mm dust) can only rule out activity at unrealistically large heliocentric distances (> 1000 au) or with unusual strength (Ye et al. 2017).

The search for gas emission from ‘Oumuamua was not comprehensive owing to the challenging observing circumstances. There were no observations that could have made sensitive enough detections of water outgassing to test for comet-like activity. The relative abundance of CN to H_2O of ‘Oumuamua needed to reconcile the non-detections of CN (Ye et al. 2017) with the inferred H_2O outgassing rate needed to account for non-gravitational forces (Micheli et al. 2018), while unusual, is not unprecedented. ‘Oumuamua needed to be depleted in CN by at least a factor of 15 relative to typical abundances in comets, while comets C/1988 Y1 Yanaka (Fink 1992) and 96P/Machholz 1 (Langland-Shula & Smith 2007; Schleicher 2008) were depleted by factors of 25 and 72, respectively. One of these highly depleted comets, 96P, also has a very low amount of dust observed at visible wavelengths compared to gas (Schleicher 2008), like ‘Oumuamua.

The upper limits to the CO and CO_2 production rates (Trilling et al. 2018 and M. Mommert priv. comm.) combined with the inferred H_2O production rate imply abundances of $CO/H_2O \leq 2\%$ and $CO_2/H_2O \leq 0.2\%$. This CO upper limit is within the range of measurements for known comets, while the CO_2 upper limit is about an order of magnitude lower (A’Hearn et al. 2012). However, CO_2 is difficult to measure, so the known sample may be biased to higher abundances. Both CO and CO_2 are much more volatile than H_2O, resulting in a trend to lower ratios with smaller heliocentric distances (Ootsubo et al. 2012). The volatility difference would have resulted in CO and CO_2 being depleted deeper than H_2O. Thus, ‘Oumuamua may have lost most/all of its CO and CO_2 prior to the observations that would have constrained their abundances. Alternatively, it may have had intrinsically low abundances of CO and CO_2 due to formation conditions in its home system. The range of these ratios of volatiles in comets has recently been found to be far greater than was previously known: C/2016 R2 PanSTARRS has CO/H_2O at least several orders of magnitude higher than any other measured comet, with no H_2O yet conclusively detected (Biver et al. 2018; Opitom et al. 2019).

Thermal models show that ices may exist within just ~ 30 cm of the surface without being released during ‘Oumuamua’s perihelion passage (Fitzsimmons et al. 2018; Seligman & Laughlin 2018). A natural consequence would be a thermal lag in which outgassing begins significantly later. Such a scenario would decrease the total amount of volatile material needed to explain the observed non-gravitational acceleration and shorten the timescale over which torques were at work (see §3.2). One thermal model was shown to be consistent with the observed non-gravitational acceleration by assuming outgassing from water in combination with another volatile species (Micheli et al. 2018).

Based on the lack of detected activity, Raymond et al. (2018a) suggested ‘Oumuamua had repeated passages close to its host star before being ejected. Such repeated close passages can remove volatiles from planetesimals’ surfaces and render ejected planetesimals inactive, or *extinct* (Rickman et al. 1991). Models that match the various distributions of Solar System comets (Nesvorný et al. 2017) predict that smaller objects become inactive more quickly, so it could

simply be that 100-m scale ejected objects like ‘Oumuamua are devolatilized in their outer layers. There could very well be a population of inactive small objects from our own Oort cloud that goes undetected because of their lack of activity, as evidenced by the Manx objects (Meech et al. 2016).

Micheli et al. (2018) considered, but ultimately rejected, a number of possible explanations for the observed non-gravitational acceleration besides cometary outgassing. Most prominently was solar radiation pressure, which required ‘Oumuamua’s density to be 3–4 orders of magnitude lower than that of asteroids of similar size (solar radiation pressure effects have been detected on a few small asteroids, e.g., Micheli et al. 2012, Micheli et al. 2013). Alternate explanations in support of solar radiation pressure have suggested that ‘Oumuamua had a low density due to a fractal aggregate structure produced either by devolatilization of a comet-like body prior to its discovery (Sekanina & Kracht 2018; Sekanina 2019) or having formed as a very large aggregate of icy dust particles beyond the snow line in its home system (Moro-Martín 2019b). Such extended, extremely low density objects have never been detected, but might naturally explain some other phenomena observed for disrupting comets (Sekanina & Kracht 2018) or help reconcile some aspects of protoplanetary disc models (Moro-Martín 2019b).

2.5. *Alien technology?*

The idea of ‘Oumuamua as alien technology has been advocated in a series of papers by Loeb and collaborators (Loeb 2018; Bialy & Loeb 2018; Siraj & Loeb 2019). While their proposed solar sail has merit for fitting some aspects of the observations — the basic idea of ‘Oumuamua having a highly flattened shape was previously considered by Belton et al. (2018) and Micheli et al. (2018) — it appears unable to explain other key aspects of the observations, and some arguments in favor of this hypothesis are simply wrong.

The key argument against the solar sail hypothesis is ‘Oumuamua’s light curve amplitude. In order for a solar sail to cause the observed non-gravitational acceleration, it needs to remain properly oriented towards the Sun. However, in order to yield the observed brightness variations, its orientation would need to be varying as viewed from Earth. Furthermore, since the actual dimensions of the solar sail would be $> 10:1$, the orientation as viewed from Earth would need to be very nearly edge on, and remain so throughout the observations despite viewing geometry changes. It has not been shown that an orientation exists that can achieve all of these constraints imposed by the observational data. Furthermore, as discussed earlier, the shape of ‘Oumuamua’s light curve, with broad maxima and narrow minima, is consistent with an elongated ellipsoid.

Loeb (2018) incorrectly claimed that ‘Oumuamua must be at least ten times “shinier” than all Solar System asteroids to make the *Spitzer Space Telescope* data consistent with the ground based observations. The *Spitzer* observations are consistent with geometric albedos $0.01 \leq p_v \leq 0.5$ (Trilling et al. 2018), with a most likely albedo of $p_v \sim 0.1$. Comets have geometric albedos of $p_v = 0.02 - 0.07$ (Kokotanekova et al. 2017, and references therein), carbonaceous and silicate asteroids have $p_v = 0.05 - 0.21$, and the most reflective asteroids have $p_v \sim 0.5$ (Thomas et al. 2011; Mainzer et al. 2011). Thus ‘Oumuamua’s measured reflectivity of ~ 0.1 is entirely consistent with normal Solar System small bodies.

Finally, based on its “unusual” kinematics and presumed scarcity, Bialy & Loeb (2018) argued that ‘Oumuamua was deliberately sent toward Earth. While provocative, this argument is baseless. First, ‘Oumuamua’s trajectory is consistent with predictions by Engelhardt et al. (2017) for *detectable* inactive ISOs (see Fig. 4 and discussion in §2.3). Second, as demonstrated in §2.2, the measured number density cannot be claimed to be at odds with expectations because of our ignorance of the size distribution of ISOs.

Thus, we find no compelling evidence to favor an alien explanation for ‘Oumuamua.

3. OPEN QUESTIONS

We have discussed the many aspects of ‘Oumuamua’s properties that can be explained naturally. However, there remain several unanswered questions regarding ‘Oumuamua that warrant further study.

3.1. *Shape*

While several models have been proposed to explain ‘Oumuamua’s very elongated shape, none can naturally match such an extreme axis ratio (of at least 6:1) within a self-consistent framework. One model (Katz 2018) invokes the complete fluidization of a planetesimal by an evolving red giant star, causing the object to assume the shape of a high angular momentum Jacobi ellipsoid. Other models have proposed that ‘Oumuamua is a fragment of a planetesimal (Raymond et al. 2018a; Rafikov 2018; Sekanina 2019) or planet (Ćuk 2018) that was tidally disrupted after a very

close passage to a low-mass star, white dwarf, or giant planet, or simply as it neared perihelion. It remains to be demonstrated whether such disruption events create fragments as stretched-out as ‘Oumuamua appears to be. A third model proposes that a large number of high-velocity impacts with dust grains may create sharp edges and planar surfaces on small bodies (Domokos et al. 2009) or simply erode enough material to substantially increase the axis ratio of small objects (Vavilov & Medvedev 2019), while a fourth proposes that it formed from a low speed collision between two ∼50 m planetesimals in a protoplanetary disk (Sugiura et al. 2019). In the context of these models, it remains to be understood why such extreme shapes are so rare among larger Solar System bodies.

3.2. *Rotation state*

The ensemble of published photometry reveals that ‘Oumuamua is in non-principal axis rotation (NPA; Fraser et al. 2018; Drahus et al. 2018; Belton et al. 2018), which is a spin state commonly observed among asteroids, including objects as small as ‘Oumuamua (Pravec et al. 2005). The details of the NPA are non-unique from the available data, including when ‘Oumuamua achieved NPA rotation. Disruption or strong gravitational encounters could have created the NPA state, and the $> 10^{11}$ yr damping timescale is sufficiently long that the tumbling may originate in or during departure from its home system (Fraser et al. 2018; Drahus et al. 2018; Belton et al. 2018; Kwiecinski et al. 2018). Alternatively, the NPA rotation might have occurred during ‘Oumuamua’s journey through our system. Rafikov (2018) argued that the level of outgassing needed to explain the non-gravitational acceleration would have resulted in a rapid change in rotation period. Even a small asymmetry in the torquing might have perturbed ‘Oumuamua from simple rotation to NPA rotation.

Rafikov (2018) found that if the large non-gravitational acceleration was caused by typical cometary outgassing, then the associated torques should have caused ‘Oumuamua to rapidly spin up beyond its rotational break up limit. In contrast, Seligman et al. (2019) showed that outgassing activity that followed the subsolar point of an elongated body could produce the observed non-gravitational acceleration and would naturally result in NPA rotation with a lightcurve amplitude and period comparable to the observations, without causing extreme spin up.

The orientation of ‘Oumuamua’s rotational angular momentum vector is unconstrained from the finite available data, but is critical for properly assessing the shape from the light curve. Belton et al. (2018) showed that the rotation can be in one of five different modes, and if it is closest to its lowest rotational energy the shape can resemble the elongated “cigar-like” shape, and only in the highest energy state would it be an “extremely oblate spheroid”. The “cigar-like” shape is the more likely configuration, both because it is energetically more stable and because it permits a much larger range of orientations on the sky (as discussed in §2.5, a very flat shape requires a very specific orientation to produce the observed light curve).

3.3. *Home system*

In spite of many attempts to trace the orbit of ‘Oumuamua back to its home system (Bailer-Jones et al. 2018; Zuluaga et al. 2018; Dybczyński & Królikowska 2018; Zhang 2018) or star cluster (Gaidos 2018; Feng & Jones 2018), no convincing candidate origin star systems or stellar associations have been identified. Whether tracing back to a unique origin is feasible depends on how long ago ‘Oumuamua was ejected from its home system, since more distant regions must be considered for longer travel times, and whether it had past encounters, since each effectively erases its dynamical past. Although future data releases of high precision surveys like Gaia are likely to spur deeper searches and may yet reveal plausible candidates, it is likely that no system will be definitively shown to be ‘Oumuamua’s origin.

In addition to travel time, uncertainties in velocity/acceleration affect our ability to identify its home system. The first generation of searches (Gaidos 2018; Feng & Jones 2018; Zuluaga et al. 2018; Dybczyński & Królikowska 2018; Zhang 2018) were based on the Keplerian orbit solution available at the time, while Bailer-Jones et al. (2018) utilized the solution that included non-gravitational acceleration, assuming that it was symmetric pre- and post-perihelion. Whether this assumption is justified is ultimately unknown as no pre-perihelion observations are available, but it is likely that outgassing was delayed due to a thermal lag (Fitzsimmons et al. 2018). Without observational constraints, the parameter space to search for a home system increases considerably.

4. CONCLUSIONS

As the first interstellar visitor to our solar system, ‘Oumuamua has challenged many of our assumptions about what small bodies from another star system would look like. While ‘Oumuamua presents a number of compelling questions, we have shown that each can be answered by assuming ‘Oumuamua to be a natural object. While it is extremely

exciting to speculate about a wide range of possibilities, the process of science requires testing hypotheses. We conclude that assertions that 'Oumuamua may be artificial are not justified when the wide body of current knowledge about solar system minor bodies and planetary formation is considered.

The Large Synoptic Survey Telescope (LSST) is expected to begin full operations in 2022 and is predicted to discover on the order of one ISO per year (Cook et al. 2016; Trilling et al. 2017; Seligman & Laughlin 2018). Thus, we will soon have a much better understanding of how common — or rare — the properties of 'Oumuamua are. This knowledge will yield great insight into the planetesimal formation, evolution, and ejection processes at work across the Galaxy.

DATA AVAILABILITY

The authors declare that the main data supporting the findings of this study are available within the article and its Supplementary Information files. Extra data are available from the corresponding author upon request.

ACKNOWLEDGEMENTS

We thank the International Space Science Institute (ISSI Bern), which made this collaboration possible. AF, MB and CS acknowledge support from UK Science and Technology Facilities Council grants ST/P0003094/1 and ST/L004569/1. KJM acknowledges support through NSF awards AST1617015, in addition to support for HST programs GO/DD-15405 and -15447 provided by NASA through a grant from the Space Telescope Science Institute, which is operated by the Association of Universities for Research in Astronomy under NASA contract NAS 5-26555. QY is supported by the GROWTH project funded by the National Science Foundation under Grant No. 1545949. This research was partially supported by the project 2015/17/B/ST9/01790 funded by the National Science Centre in Poland. MMK acknowledges support from NASA Near Earth Object Observations grant #NNX17AK15G. AGL acknowledges funding from the European Research Council (ERC) under grant agreement No 802699. AM and DET are supported in part by Spitzer/NASA through an award issued by JPL/Caltech. SNR acknowledges helpful discussions with Phil Armitage related to the ISO number/mass density, and the Virtual Planetary Laboratory research team, funded by the NASA Astrobiology Program under NASA Grant Number 80NSSC18K0829. This work benefited from participation in the NASA Nexus for Exoplanet Systems Science research coordination network.

AUTHOR CONTRIBUTIONS

MMK and AF organized the ISSI team. KJM created Figures 1 & 2, SNR conducted the modelling of inferred ISO number density and created Figure 3. MMK, AF, and RJ created Figure 4 from source data provided by T. Engelhardt. All authors discussed the topics in the paper, contributed to the writing, and commented on the manuscript at all stages.

COMPETING INTERESTS

The authors declare no competing financial interests.

REFERENCES

Adams, F. C., Proszkow, E. M., Fatuzzo, M., & Myers, P. C. 2006, ApJ, 641, 504

A'Hearn, M. F., Millis, R. C., Schleicher, D. O., Osip, D. J., & Birch, P. V. 1995, Icarus, 118, 223

A'Hearn, M. F., Belton, M. J. S., Delamere, W. A., et al. 2011, Science, 332, 1396

A'Hearn, M. F., Feaga, L. M., Keller, H. U., et al. 2012, ApJ, 758, 29

Almeida-Fernandes, F., & Rocha-Pinto, H. J. 2018, MNRAS, 480, 4903

Anguiano, B., Majewski, S. R., Freeman, K. C., Mitschang, A. W., & Smith, M. C. 2018, MNRAS, 474, 854

Bailer-Jones, C. A. L., Farnocchia, D., Meech, K. J., et al. 2018, AJ, 156, 205

Bannister, M. T., Schwamb, M. E., Fraser, W. C., et al. 2017, ApJ, 851, L38

Belton, M. J. S., Hainaut, O. R., Meech, K. J., et al. 2018, ApJL, 856, L21

Bhandare, A., Breslau, A., & Pfalzner, S. 2016, A&A, 594, A53

Bialy, S., & Loeb, A. 2018, ApJ, 868, L1

Biver, N., Bockelée-Morvan, D., Paubert, G., et al. 2018, A&A, 619, A127

Bolin, B. T., Weaver, H. A., Fernandez, Y. R., et al. 2018, ApJL, 852, L2

Bovy, J. 2017, MNRAS, 470, 1360

Burgasser, A. J., Logsdon, S. E., Gagné, J., et al. 2015, ApJS, 220, 18

Cassan, A., Kubas, D., Beaulieu, J.-P., et al. 2012, Nature, 481, 167

Charnoz, S., & Morbidelli, A. 2003, Icarus, 166, 141

Clanton, C., & Gaudi, B. S. 2016, ApJ, 819, 125

Coşkunoğlu, B., Ak, S., Bilir, S., et al. 2011, MNRAS, 412, 1237

Cook, N. V., Ragozzine, D., Granvik, M., & Stephens, D. C. 2016, ApJ, 825, 51

Cowan, J. J., & A'Hearn, M. F. 1979, Moon and Planets, 21, 155

Ćuk, M. 2018, ApJL, 852, L15

Do, A., Tucker, M. A., & Tonry, J. 2018, ApJL, 855, L10

Dohnanyi, J. S. 1969, J. Geophys. Res., 74, 2531

Domokos, G., Sipos, A. Á., Szabó, G. M., & Várkonyi, P. L. 2009, ApJL, 699, L13

Drahus, M., Guzik, P., Waniak, W., et al. 2018, Nature Astronomy, 2, 407

Dybczyński, P. A., & Królikowska, M. 2018, A&A, 610, L11

Engelhardt, T., Jedicke, R., Vereš, P., et al. 2017, AJ, 153, 133

Feng, F., & Jones, H. R. A. 2018, ApJL, 852, L27

Fink, U. 1992, Science, 257, 1926

Fitzsimmons, A., Snodgrass, C., Rozitis, B., et al. 2018, Nature Astronomy, 2, 133

Ford, E. B., & Rasio, F. A. 2008, ApJ, 686, 621

Fraser, W. C., Pravec, P., Fitzsimmons, A., et al. 2018, Nature Astronomy, 2, 383

Fujiwara, A., Kawaguchi, J., Yeomans, D. K., et al. 2006, Science, 312, 1330

Gaidos, E. 2018, MNRAS, 477, 5692

Haisch, Karl E., J., Lada, E. A., & Lada, C. J. 2001, ApJ, 553, L153

Hands, T. O., Dehnen, W., Gration, A., Stadel, J., & Moore, B. 2019, arXiv e-prints, arXiv:1901.02465

Hernández, J., Hartmann, L., Calvet, N., et al. 2008, ApJ, 686, 1195

Holman, M. J., & Wiegert, P. A. 1999, AJ, 117, 621

Izidoro, A., Morbidelli, A., Raymond, S. N., Hersant, F., & Pierens, A. 2015, A&A, 582, A99

Jackson, A. P., Tamayo, D., Hammond, N., Ali-Dib, M., & Rein, H. 2018, MNRAS, 478, L49

Jewitt, D., Agarwal, J., Hui, M.-T., et al. 2018, ArXiv e-prints, arXiv:1811.07180

Jewitt, D., Luu, J., Rajagopal, J., et al. 2017, ApJ, 850, L36

Johnson, J. A., Butler, R. P., Marcy, G. W., et al. 2007, ApJ, 670, 833

Katz, J. I. 2018, MNRAS, 478, L95

Knight, M. M., Protopapa, S., Kelley, M. S. P., et al. 2017, ApJL, 851, L31

Kokotanekova, R., Snodgrass, C., Lacerda, P., et al. 2017, MNRAS, 471, 2974

Kresak, L. 1992, A&A, 259, 682

Krivov, A. V. 2010, Research in Astronomy and Astrophysics, 10, 383

Kroupa, P., Tout, C. A., & Gilmore, G. 1993, MNRAS, 262, 545

Kwiecinski, J. A., Krause, A. L., & Van Gorder, R. A. 2018, Icarus, 311, 170

Lacerda, P., & Jewitt, D. C. 2007, AJ, 133, 1393

Langland-Shula, L. E., & Smith, G. H. 2007, ApJL, 664, L119

Laplace, P.-S. 1812, Théorie analytique des probabilités

Lisse, C. M., Fernández, Y. R., A'Hearn, M. F., et al. 2004, Icarus, 171, 444

Loeb, A. 2018, ArXiv e-prints, arXiv:1811.08832

Lovis, C., & Mayor, M. 2007, A&A, 472, 657

Lowry, S. C., Fitzsimmons, A., Pravec, P., et al. 2007, Science, 316, 272

Mainzer, A., Grav, T., Masiero, J., et al. 2011, ApJ, 741, 90

Masiero, J. 2017, arXiv e-prints, arXiv:1710.09977

Mayor, M., Marmier, M., Lovis, C., et al. 2011, arXiv e-prints, arXiv:1109.2497

McGlynn, T. A., & Chapman, R. D. 1989, ApJL, 346, L105

McNeill, A., Trilling, D. E., & Mommert, M. 2018, ApJL, 857, L1

Meech, K. J., & Svoren, J. 2004, Using cometary activity to trace the physical and chemical evolution of cometary nuclei, ed. G. W. Kronk, 317–335

Meech, K. J., Yang, B., Kleyna, J., et al. 2016, Science Advances, 2, e1600038

Meech, K. J., Weryk, R., Micheli, M., et al. 2017, Nature, 552, 378

Micheli, M., Tholen, D. J., & Elliott, G. T. 2012, NewA, 17, 446

—. 2013, Icarus, 226, 251

Micheli, M., Farnocchia, D., Meech, K. J., et al. 2018, Nature, 559, 223

Montesinos, B., Eiroa, C., Krivov, A. V., et al. 2016, A&A, 593, A51

Moretti, P. F., Maras, A., & Folco, L. 2007, Advances in Space Research, 40, 258

Moro-Martín, A. 2018, ApJ, 866, 131

—. 2019a, AJ, 157, 86

—. 2019b, ApJL, 872, L32

Moro-Martín, A., Turner, E. L., & Loeb, A. 2009, ApJ, 704, 733

Nesvorný, D., Vokrouhlický, D., Dones, L., et al. 2017, ApJ, 845, 27

Ootsubo, T., Kawakita, H., Hamada, S., et al. 2012, ApJ, 752, 15

Opitom, C., Hutsemékers, D., Jehin, E., et al. 2019, arXiv e-prints, arXiv:1901.00657

Pajola, M., Vincent, J.-B., Güttler, C., et al. 2015, A&A, 583, A37

Park, R. S., Pisano, D. J., Lazio, T. J. W., Chodas, P. W., & Naidu, S. P. 2018, AJ, 155, 185

Pätzold, M., Andert, T. P., Hahn, M., et al. 2018, MNRAS, doi:10.1093/mnras/sty3171

Pfalzner, S., Steinhausen, M., & Menten, K. 2014, ApJ, 793, L34

Pfalzner, S., Vogel, P., Scharwächter, J., & Olczak, C. 2005, A&A, 437, 967

Polishook, D., Moskovitz, N., DeMeo, F. E., & Binzel, R. P. 2014, Icarus, 243, 222

Portegies Zwart, S., Torres, S., Pelupessy, I., Bédorf, J., & Cai, M. X. 2018, MNRAS, 479, L17

Pravec, P., Harris, A. W., Scheirich, P., et al. 2005, Icarus, 173, 108

Rafikov, R. R. 2018, ApJL, 867, L17

Raymond, S. N., Armitage, P. J., & Gorelick, N. 2010, ApJ, 711, 772

Raymond, S. N., Armitage, P. J., & Veras, D. 2018a, ApJL, 856, L7

Raymond, S. N., Armitage, P. J., Veras, D., Quintana, E. V., & Barclay, T. 2018b, MNRAS, 476, 3031

Raymond, S. N., & Izidoro, A. 2017, Icarus, 297, 134

Reach, W. T., Sykes, M. V., Lien, D., & Davies, J. K. 2000, Icarus, 148, 80

Rickman, H., Kamel, L., Froeschle, C., & Festou, M. C. 1991, AJ, 102, 1446

Roell, T., Neuhäuser, R., Seifahrt, A., & Mugrauer, M. 2012, A&A, 542, A92

Sagan, C. 1979, Broca's Brain : Reflections on the Romance of Science

Schäfer, U., Yang, C.-C., & Johansen, A. 2017, A&A, 597, A69

Schleicher, D. G. 2008, AJ, 136, 2204

Sekanina, Z. 1982, AJ, 87, 161

—. 2019, arXiv e-prints, arXiv:1901.08704

Sekanina, Z., & Kracht, R. 2018, arXiv e-prints, arXiv:1812.07054

Seligman, D., & Laughlin, G. 2018, AJ, 155, 217

Seligman, D., Laughlin, G., & Batygin, K. 2019, arXiv e-prints, arXiv:1903.04723

Simon, J. B., Armitage, P. J., Youdin, A. N., & Li, R. 2017, ApJL, 847, L12

Siraj, A., & Loeb, A. 2019, Research Notes of the American Astronomical Society, 3, 15

Sugiura, K., Kobayashi, H., & Inutsuka, S.-i. 2019, arXiv e-prints, arXiv:1903.06373

Suzuki, D., Bennett, D. P., Sumi, T., et al. 2016, ApJ, 833, 145

Taylor, P. A., Margot, J.-L., Vokrouhlický, D., et al. 2007, Science, 316, 274

Thebault, P., & Haghighipour, N. 2015, Planet Formation in Binaries, ed. S. Jin, N. Haghighipour, & W.-H. Ip, 309–340

Thomas, C. A., Trilling, D. E., Emery, J. P., et al. 2011, AJ, 142, 85

Tremaine, S. 1993, in Planets Around Pulsars, ed. J. A. Phillips, S. E. Thorsett, & S. R. Kulkarni, Vol. 36, 335–344

Trilling, D. E., Bryden, G., Beichman, C. A., et al. 2008, ApJ, 674, 1086

Trilling, D. E., Robinson, T., Roegge, A., et al. 2017, ApJL, 850, L38

Trilling, D. E., Mommert, M., Hora, J. L., et al. 2018, AJ, 156, 261

Vavilov, D. E., & Medvedev, Y. D. 2019, MNRAS, arXiv:1812.11334

Veras, D. 2016, Royal Society Open Science, 3, 150571

Veras, D., Wyatt, M. C., Mustill, A. J., Bonsor, A., & Eldridge, J. J. 2011, MNRAS, 417, 2104

Vincke, K., & Pfalzner, S. 2016, ApJ, 828, 48

Warner, B. D., Harris, A. W., & Pravec, P. 2009, Icarus, 202, 134

Williams, G. V., Sato, H., Sarneczky, K., et al. 2017a, Central Bureau Electronic Telegrams, 4450, 1

Williams, G. V., Bacci, P., Maestripieri, M., et al. 2017b, Minor Planet Electronic Circulars, 2017-U181

Winn, J. N., & Fabrycky, D. C. 2015, ARA&A, 53, 409

Wyatt, M. C. 2008, ARA&A, 46, 339

Ye, Q.-Z., & Hui, M.-T. 2014, ApJ, 787, 115

Ye, Q.-Z., Zhang, Q., Kelley, M. S. P., & Brown, P. G. 2017, ApJL, 851, L5

Zappala, V., Cellino, A., Barucci, A. M., Fulchignoni, M., & Lupishko, D. F. 1990, A&A, 231, 548

Zhang, Q. 2018, ApJL, 852, L13

Zhang, S., Zhu, Z., Huang, J., et al. 2018, ApJL, 869, L47

Zuluaga, J. I., Sánchez-Hernández, O., Sucerquia, M., & Ferrín, I. 2018, AJ, 155, 236